JOURNAL OF SPACECRAFT AND ROCKETS
Vol. 47, No. 1, January–February 2010

Aerodynamic Analysis of a Spinning Missile Using a High-Order Unstructured-Grid Scheme

Chunhua Sheng,* Xiao Wang,† and Qiuying Zhao‡
Mississippi State University, Mississippi State, Mississippi 39762

DOI: 10.2514/1.42988

Time-accurate viscous flow simulations are carried out for a canard-controlled missile in which the missile body spins at a constant roll rate while the canards are dithering. Unsteady Reynolds-averaged Navier–Stokes equations are solved using an arbitrary Mach number algorithm based on unstructured-grid topology and embedded dynamic moving-grid technique for complex missile configuration with movable control surfaces. A new higher-order flux reconstruction scheme is investigated and compared with the original second-order scheme for resolving the complicated flowfield associated with the missile control surfaces (canards). The numerical simulations revealed the formation of a pair of counter-rotating vortices induced by each canard, which interact with the tail fin shocks and boundary layers on the body. A grid refinement study is carried out to assess the efficacy of the high-order spatial discretization in resolving vortex-dominant flows. The computational results show that the higher-order flux reconstruction method introduced in the present study noticeably reduces the numerical dissipation of vortical flows encountered by the conventional second-order schemes and thus significantly reduces the computational costs for the aerodynamic simulation of the spinning missile.

Nomenclature

C_F	=	force coefficient, force$/Q_\infty S_{\text{ref}}$
C_M	=	force coefficient, moment$/Q_\infty S_{\text{ref}} L_{\text{ref}}$
e_t	=	total energy
F	=	vector of inviscid and viscous fluxes
L	=	length of the missile body
L_{ref}	=	reference length, maximum body diameter
M	=	transformation matrix
M_r	=	freestream Mach number
$\hat{\boldsymbol{n}}$	=	control volume unit normal vector, $(n_x, n_y, n_z)^T$
p	=	static pressure
q	=	vector of primitive variables, $(\rho, u, v, w, p)^T$
Q	=	vector of conservative variables, $(\rho, \rho u, \rho v, \rho w, e_t)^T$
Q_∞	=	freestream dynamic pressure, $\frac{1}{2}\rho_\infty U_\infty^2$
r	=	position vector
S_{ref}	=	reference area, cross-sectional area at maximum body diameter
t	=	time
U_∞	=	freestream velocity
β	=	preconditioning parameter
Γ_q^{-1}	=	preconditioning matrix
ρ	=	fluid density
Ω	=	rotational speed of relative frame or control volume

Subscripts

L	=	left side of the face of a control volume
R	=	right side of the face of a control volume

Presented as Paper 1090 at the the 47th AIAA Aerospace Sciences Meeting, Orlando, FL, 5–8 January 2009; received 15 January 2009; revision received 4 September 2009; accepted for publication 23 September 2009.

*Center for Advanced Vehicular Systems; currently Associate Professor of Mechanical Engineering, University of Toledo. Associate Fellow AIAA.
†Assistant Research Professor, Center for Advanced Vehicular Systems.
‡Graduate Research Assistant, Center for Advanced Vehicular Systems.

Introduction

THE aerodynamics of a rolling airframe missile are characterized by multiple shocks and highly unsteady and vortical flows, which interact with the tail fins and body boundary layers. Numerical simulation of a rolling missile with dithering canards poses significant challenges for any computational fluid dynamics (CFD) solvers. Not only does the solver need to accurately predict the location and strength of shocks and vortices generated by the missile control surfaces and sharp edges, but it also needs to capture the fast dynamic responses of the missile motion associated with the dithering canards. In the past several years, a number of researchers have attempted to use different approaches to predict and analyze the aerodynamic performance of this missile configuration. Nygaard and Meakin [1,2] used an overset structured-grid approach to perform the Euler and Navier–Stokes computations with a series of refined meshes and assessed viscous effects on the aerodynamic forces. Their results showed that a finer mesh increased the accuracy of drag prediction and had a great effect on the aerodynamic loading prediction. Blades et al. [3,4] performed similar calculations using an unstructured-grid scheme for compressible flows to predict the aerodynamic performance of the spinning missile. They used a sliding interface [5] method to account for the motion of dithering canards and obtained the aerodynamic forces and moments that were compatible with the OVERFLOW results [2]. Later, Sheng et al. [6] used an arbitrary Mach number flow solver to predict the rolling missile configuration with fixed canards. This particular version of the U^{2}NCLE solver [7] has showed a superior stability and robustness compared to its compressible flow version counterpart [3]. An extensive aerodynamic performance database has been generated for the spinning missile with deflected canards (0, ±15, and ±30 deg) in a range of Mach numbers (0.8 to 2.2) and angles of attack (0 to 12 deg) [6], which was the first time that such a large aerodynamic performance database was solely derived from the unsteady viscous simulations in the missile trajectory prediction.

In the current work, a rolling airframe missile with dithering canards is numerically investigated using a new higher-order flux reconstruction scheme of the arbitrary Mach number U^{2}NCLE solver [7,8]. A robust dynamic moving-grid technique [9] was adopted to handle the relative motion between the dithering canards and rolling airframe. Note that unsteady simulations of the spinning missile, which has dithering canards sweeping between two extremes at high rates, remain a technical challenge even for the conventional second-order schemes, not to mention the higher-order scheme, due to less numerical dissipations. An efficient higher-order inviscid flux

reconstruction method combined with a limiter-detector technique [10] is introduced for the improved prediction of vortical flows induced by the dithering canards of a rolling missile. The numerical results are compared with the original scheme on the aerodynamic prediction of forces and moments, induced vortex convection, and interaction of the vortex with the boundary layer. Predicted aerodynamic force and moment coefficients are also compared with the benchmark results obtained by NASA OVERFLOW code [1,2].

Missile Configuration and Computational Mesh

The missile configuration [11] considered in this study contains a hemispherical nose, cylindrical midbody, and a boattail forward of an additional cylindrical aftbody, two dithering canards located aft of the nose, and four fixed tail fins located behind the boattail on the most aft cylindrical section (see Fig. 1). The tail fins are slightly canted to impart a roll to the airframe. The two canards act as control surfaces and are interconnected, and thus their motion is synchronous. In the simulations of a spinning body and dithering canards, the canards sweep between the extremes. The canard actuator flips back and forth between the two extremes over a missile roll revolution. The missile spins at a constant roll rate. To model the complex motions of the spinning missile and the dithering canards, an embedded dynamic moving-grid technique [9] with nested parent and child volumes are used. In this approach, the absolute motion of the canards is considered as a combination of the dithering motion relative to the missile body and the spinning motion of the missile. Therefore, a child moving-volume grid is created around the canards, as shown in Fig. 1 to model the canard dithering, and a parent moving grid is constructed around the entire missile to handle the spinning motion. The mixed-element-type unstructured grid was generated to be suitable for viscous simulations. The volume grid is constructed using the advancing-front local-reconnection grid generation technique [12]. SolidMesh [13] was used to prepare the CAD geometry and generate the surface grids.

In order to resolve the vortical flows generated by the canards and their convection along the missile body, an embedded interior surface is constructed around the missile. This interior surface is used to control the point spacing and the cell growth in the vicinity of the missile body. It allows effective use of grid points that are distributed to important flow regions without global grid refinements. The embedded surface encapsulates the entire missile body, canard, and tail fin surfaces, and its maximum radial span is about two diameters of the missile body. By adjusting the grid spacing on the embedded surface, the volume grid resolution can be easily controlled.

In this work, grid resolution studies are conducted to evaluate its impact on the simulation of vortical flows and the efficacy/costs of the new higher-order scheme. A baseline coarse grid is generated containing 9.26 million nodes and 34.53 million mixed elements. A second refined grid is generated by doubling the number of grid points on the embedded surface, which results in a volume mesh with 17.02 million nodes and 72.62 million mixed elements. Figure 2 shows the cutting planes on the coarse and fine grids through the canard surfaces at an axial station measured 0.145 body lengths from the missile nose. The impact of the grid refinement on the flowfield simulation will be discussed in the Results section.

For the viscous grid, the normal spacing of the first grid point from the solid surface is 4.06×10^{-5}, based on the length of the missile body, which leads to a y^+ distribution of about 1.0 over all the solid surfaces and ensures good viscous-sublayer resolution. The outer far-field boundary of the computational domain is a sphere with a diameter of 3.67 body lengths of the missile.

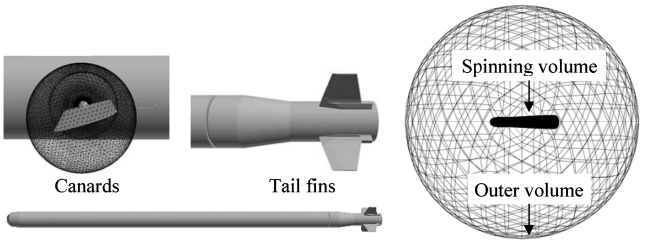

a) Missile geometry with tail fins and movable canards **b) Missile spinning volumes**

Fig. 1 Missile geometry and computational model.

Numerical Methods

In the following, the governing equations and numerical methods for the arbitrary Mach number solution algorithm are described first, followed by a brief description of the higher-order inviscid flux reconstruction method introduced in the present work. Since the focus of the current study is to apply the new flux reconstruction scheme to predict the complex and vortical flows of the spanning missile with dithering canards and to assess the efficacy and benefit of the proposed method over the conventional second-order scheme, detailed derivation of the numerical flux scheme as well as the verification of formal order of accuracy will not be provided in the current paper, which will be published later in a separate paper.

Primitive Variable Formulation

The unsteady three-dimensional compressible Reynolds-averaged Navier–Stokes equations are cast in a Cartesian coordinate system and are written in a finite volume form. It represents a system of conservation laws for a control volume that relates the rate of change of a vector of average state variables to the flux through the face of a control volume. The conservative flux formulation is written in terms of primitive variables for the preconditioning purpose in order to compute flows at arbitrary Mach numbers. The primitive variable formulation of the governing equation, after introducing a preconditioning matrix Γ_q^{-1} [14], can be expressed as

$$\boldsymbol{M}\,\Gamma_q^{-1}\frac{\partial}{\partial \boldsymbol{t}}\int_{\Omega}\boldsymbol{q}\,\mathrm{d}\boldsymbol{V}+\oint_{\partial\Omega}\boldsymbol{F}\cdot\mathbf{n}\,\mathrm{d}\boldsymbol{A}=0 \tag{1}$$

where Γ_q^{-1} is a constant diagonal preconditioning matrix that only depends on the global reference Mach number M_r,

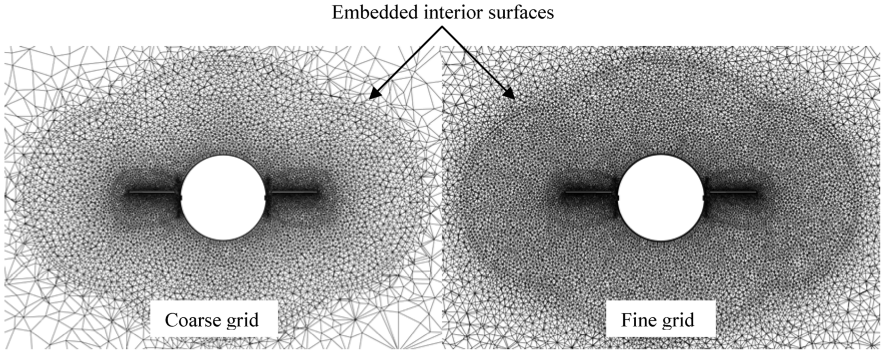

Fig. 2 Coarse- and fine-grid resolutions on the cutting plane at $x/L = 0.145$.

$$\Gamma_q^{-1} = \mathrm{diag}[\,1, \quad 1, \quad 1, \quad 1, \quad 1/\beta(M_r)\,]$$
$$\beta(M_r) = M_r^{\lambda} \quad \lambda \in [0, 2] \tag{2}$$

$\boldsymbol{M}$ is the transformation matrix from conservative variables

$$\boldsymbol{Q} = (\,\rho, \quad \rho u, \quad \rho v, \quad \rho w, \quad \rho e_t\,)$$

to primitive variables

$$\boldsymbol{q} = (\,\rho, \quad u, \quad v, \quad w, \quad p\,)$$

and $\boldsymbol{F}$ is the vector of the flux on the face of the control volume. Since the governing equations are solved in the fixed reference frame, where the missile configuration is rolling, there is no source term (Coriolis and centrifugal forces) added into the above equation.

Inviscid Flux Approximation

Recall from [14] that preconditioned Eqs. (1) can be expressed in a differential form as

$$\boldsymbol{M}\,\Gamma_q^{-1}\frac{\partial \boldsymbol{q}}{\partial \boldsymbol{t}} + \boldsymbol{M}\Gamma_q^{-1}|\Gamma_q \boldsymbol{M}^{-1}\boldsymbol{A}\boldsymbol{M}|\frac{\partial \boldsymbol{q}}{\partial \boldsymbol{x}} = 0 \tag{3}$$

where $\Gamma_q \boldsymbol{M}^{-1}\boldsymbol{A}\boldsymbol{M}$ is the system matrix for the preconditioned equations, and $\boldsymbol{A} = \partial \boldsymbol{F}/\partial \boldsymbol{Q}$ is the flux Jacobian matrix with respect to $\boldsymbol{Q}$. For the preconditioned system, the inviscid flux approximation at the interface of the control volume is

$$\boldsymbol{F} = \frac{\mathbf{1}}{\mathbf{2}}(\boldsymbol{F}(\boldsymbol{q}_L) + \boldsymbol{F}(\boldsymbol{q}_R)) - \frac{\mathbf{1}}{\mathbf{2}}\boldsymbol{M}\Gamma_q^{-1}|\Gamma_q \boldsymbol{M}^{-1}\boldsymbol{A}\boldsymbol{M}|(\boldsymbol{q}_R - \boldsymbol{q}_L) = 0 \tag{4}$$

The eigensystem of Eq. (4) is evaluated based on the averaged variables instead of Roe variables, which is considered to be an extension of the Roe flux approximation.

In Eq. (4), quantities $\boldsymbol{q}_L$ and $\boldsymbol{q}_R$ are values of primitive variables on the left and right states of the interface of a control volume. For the first-order-accurate differencing scheme, $\boldsymbol{q}_L$ and $\boldsymbol{q}_R$ are set equal to the values at the nodes lying on either side of the interface. For the conventional second-order scheme, these values at the interface are computed with a Taylor series expansion about the central node of the control volume:

$$\boldsymbol{q}_{\text{face}} = \boldsymbol{q}_{\text{node}} + \nabla \boldsymbol{q}_{\text{node}} \cdot \mathbf{r} \tag{5}$$

where $\mathbf{r}$ is the vector that extends from the central node to the interface of the control volume, and $\nabla \boldsymbol{q}$ is the first derivatives of the primitive variables at the node that are evaluated with an unweighted least-squares procedure [15].

The above second-order numerical scheme has been used in the previous study for generating the aerodynamic performance database [6]. For the current study of the spinning missile with dithering canards, it is used to provide a baseline solution for comparison with the higher-order flux scheme, which will be described next.

Higher-Order Flux Reconstruction

There are ongoing efforts in the CFD community to develop high-order discretization schemes [16–23] due to less numerical dissipations than conventional second-order schemes. The use of higher-order schemes may be important for certain aerodynamic and acoustic applications such as helicopter rotors and missile systems, where the vortices induced by helicopter rotors and missile control surfaces have a significant impact on the aerodynamic and/or acoustic performance. The higher-order numerical schemes can better preserve the vortex trajectory and strength on moderate computational grids, avoiding the need for expensive grid adaptation and/or local grid refinement in the vicinity of vortex cores. Although notable successes have been achieved in the structured grid-based algorithms [17], development of an efficient and robust high-order discretization scheme based on unstructured grids is still a technical challenge. This challenge is mainly due to the fact that most high-order unstructured schemes encounter a large stencil and thus more computing costs or are not intuitive to understand and/or are difficult to implement [18,21]. Another major obstacle for the high-order unstructured-grid schemes is the lack of an efficient and robust limiter for practical and complex aerodynamic applications, such as the case of the spinning missile with dithering canards presented in the current work. It is very difficult to balance the requirements on numerical accuracy and stability of a high-order scheme when both strong vortices and shocks exist in the flowfield, as these two have conflicting requirements toward the numerical scheme. In the present study, an efficient and robust higher-order spatial discretization method is introduced based on an upwind-biased quadratic polynomial reconstruction of primitive variables, combined with a limiter-detector technique [10] for complex flow simulations with strong shocks.

Recall in formula (5) that a conventional second-order flux reconstruction scheme can be achieved by using a linear representation of flow variables within the control volume. In the present study, the following quadratic polynomial is used to replace the linear representation in order to develop a higher-order flux approximation:

$$\boldsymbol{q}_{\text{face}} = \boldsymbol{q}_{\text{node}} + \nabla \boldsymbol{q}_{\text{node}} \cdot \mathbf{r} + \boldsymbol{f}(\boldsymbol{q}_{\text{node}}, \nabla \boldsymbol{q}_{\text{node}})\mathbf{r}^2 \tag{6}$$

where the extra term $\boldsymbol{f}$ in Eq. (6) is to account for the high-order polynomial, which is constructed based on an upwind-biased formula using both primitive variables and their gradients to develop compact stencils:

$$\boldsymbol{f} = \frac{(\boldsymbol{q}_o - \boldsymbol{q}_i) - \nabla \boldsymbol{q}_i \cdot (\mathbf{r}_o - \mathbf{r}_i)}{(\mathbf{r}_o - \mathbf{r}_i)^2} \tag{7}$$

In Eq. (7), subscripts i and o denote the node state inside and outside of the control volume at a given boundary interface (see Fig. 3). Unlike the work of Barth and Frederickson [16] and Nejat and Ollivier-Gooch [10], in which the second derivatives of primitive variables were used in the reconstruction of a quadratic polynomial, the current method uses both primitive variables and their first derivatives of the inner node to reconstruct a quadratic polynomial, avoiding the large stencils associated with the second derivatives in each control volume. This is the major difference between the current high-order reconstruction method and the previous works [10,16]. The reconstruction of a piecewise quadratic polynomial within each control volume is essential for developing a third-order spatial discretization scheme.

If the above reconstructed piecewise-discontinuous polynomial is accurate to the degree of two, a third-order flux reconstruction scheme can be achieved at the interface of the control volume. As pointed out by Barth and Frederickson [16], an equally important factor as the high-order piecewise polynomial is the accuracy of the high-order flux integration on the interface. In order to maintain the third-order flux reconstruction scheme, a Gauss quadrature method should be applied for the surface integral within the control volume. This can be achieved by evaluating an approximate number of quadrature points for certain surface shapes (for example, three points for a triangle surface in three dimensions) evaluated based on the quadratic polynomial (6). However, due to the irregular nature of the shape of the interface for vertex-centered schemes, each interface has to be decomposed into multiple triangles that compose the interface. This would greatly increase the memory requirements and computational costs, which would otherwise be relatively easy for cell-centered schemes. An economic but less accurate way is to use

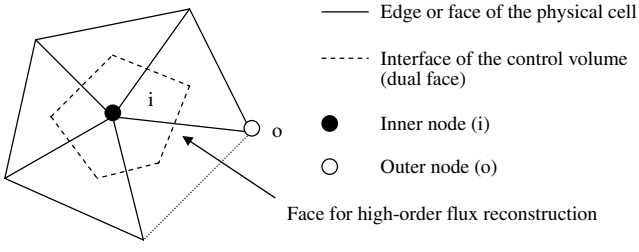

Fig. 3 Diagram of a vertex-centered scheme.

the central point only on each interface for the surface integration. Although the accuracy of the numerical scheme would be compromised in some degrees, it still showed considerable improvement in predicting the complex flowfield using the above high-order polynomial reconstruction, which will be demonstrated in the Results section.

Limiter-Detector Technique

Because of the upwind nature of the above reconstruction method [Eqs. (6) and (7)], no limiter is required if the flowfield is smooth and does not contain any discontinuities (shocks). The current high-order flux reconstruction has demonstrated an improved accuracy while maintaining the stability of the numerical solution. For flows with strong discontinuities or gradients, such as the case of supersonic flows in the spinning missile with dithering canards, the underlying numerical dissipation may not be enough to eliminate the oscillation of solutions at discontinuities. The use of a monotonic limiter becomes necessary. However, as indicated in the recent survey for high-order unstructured schemes [23], it remains one of the top technical challenges to develop an efficient limiter at discontinuities without degrading the overall accuracy of the scheme in the smooth region. In the present study, a limiter-detector technique [9] is investigated and used to maintain the high-order accuracy in the smooth region, while providing enough numerical dissipation near the discontinuity. This is achieved by applying a limiter-detector coefficient σ to the linear and quadratic parts of the reconstructed polynomial (6):

$$\bar{\boldsymbol{q}}_{\text{face}} = \boldsymbol{q}_{\text{node}} + [(1-\sigma)\phi_{\text{node}} + \sigma]\nabla \boldsymbol{q}_{\text{node}} \cdot \mathbf{r} + \sigma \boldsymbol{f}(\boldsymbol{q}_{\text{node}}, \nabla \boldsymbol{q}_{\text{node}})\mathbf{r}^2 \tag{8}$$

where $\bar{\boldsymbol{q}}$ is the reconstructed primitive variables with the limiter, and θ is any monotonic limiters. The coefficient σ is evaluated based on a formula suggested by Netjat and Ollivier-Gooch [10]. Ideally, this filter will turn off the high-order part in the flow region with strong discontinuity but will have no effect in the smooth region to achieve the maximum accuracy offered by the high-order scheme. This approach has been successfully used in the current simulation of the spinning missile with dithering canards, where both a smooth region (vortical flows) and a discontinuous region (shocks) exist in the same flowfield.

Viscous Flux Evaluation

The viscous flux discretization is still second order in the present work, as it provides secondary contribution to the overall numerical accuracy of the scheme. The current unstructured viscous grids are composed of mixed types of elements, including tetrahedron, quadrahedron, prism, and hexahedron. There are two key issues in reconstructing the viscous flux. One is the positivity of the discrete operator, which requires that all of the stencil weights be positive. Positivity is a key property for numerical stability. Another key property is the linearity-preserving of gradients (for second-order scheme). In this work, a positive scheme proposed in [7] is used to compute gradients of flow variables at the medial dual faces for stable and accurate simulations of viscous flows.

Turbulence Model

Several turbulence closure models have been developed for high-Reynolds-number flows. One of them is the Spalart–Allmaras one-equation turbulence model [24], which formulates a transport equation for the turbulence Reynolds number and is the only one used in the present study, due to its simplicity. From the original Spalart–Allmaras formulation, a transport equation for the turbulence Reynolds number $\tilde{\nu}$ (working variable) is expressed as

$$\frac{\partial \tilde{\nu}}{\partial t} + \mathbf{V}\cdot\nabla\tilde{\nu} = c_{b1}(f_{r1} - f_{t2})\tilde{S}\,\tilde{\nu} - \frac{1}{Re}\left[c_{w1}f_w - \frac{c_{b1}}{k^2}f_{t2}\right]\left[\frac{\tilde{\nu}}{d}\right]^2 + \frac{1}{\sigma Re}\{\nabla\cdot[(\tilde{\nu} + (1+c_{b2})\tilde{\nu})\nabla\tilde{\nu}] - c_{b2}\tilde{\nu}\nabla\cdot(\nabla\tilde{\nu})\} \tag{9}$$

where the first and second terms on the right-hand side of Eq. (9) are the source production, and the third term is the turbulence dissipation. Details of the coefficients in Eq. (9) can be found in [24].

Iterative Procedures

The baseline flow solver is a vertex-centered finite volume implicit scheme using unstructured mixed-element grids. The time-advancement algorithm is based on the implicit Newton's method, which yields a linear system of equations for the solution at each time step. The solution of the sparse system of equations is obtained by a symmetric Gauss–Seidel relaxation method. Normally, six to eight symmetric Gauss–Seidel realizations are adequate at each time step. For unsteady time-accurate simulations, four Newton subiterations are normally used to maintain the stability and temporal accuracy of the unsteady solutions.

Results

Unsteady Navier–Stokes simulations were performed to investigate the complex vortical flowfield and aerodynamic forces and moments for the spinning missile with dithering canards, using both the original second-order and new higher-order flux reconstruction schemes. The missile roll rate is fixed at 9 Hz in the current study. The freestream Mach number is 1.6, the Reynolds number is 41.327×10^6, and the flow angle of attack is 3 deg.

The missile uses modified proportional navigation guidance logic. The canard control surfaces are designed to perform the missile directional control by changing their pitch positions as the missile rolls. The maximum movements of the canards are ± 15 deg from the zero-deflection position. The rotation of the canards is synchronous and specified by a canard command level [11]. For a 0% command level, the canard actuator flips back and forth between its two extremes. The canard dithering rate is 36 Hz at 0% command level, and the time required for the canards to switch between the positive and negative extremes is approximately 20 deg roll angle of the body [11].

Computations of the spinning missile with dithering canards were carried out using parallel processors on a Sun X2200 M2 cluster (2048 computer cores, 2.6 GHz Opteron 2218, 4 TB of RAM) located at the High Performance Computing Collaboratory of Mississippi State University. Simulations on the baseline coarse grid were performed using 64 processors, and simulation on the fine grid was performed using 128 processors. The internode communication is through the message-passing interface (OpenMPI) operating on SUSE8 Linux operating system. A converged unsteady solution was obtained in about three missile revolutions. In the following, a comparative study is performed between the results obtained with the original and new higher-order flux schemes. Computed aerodynamic

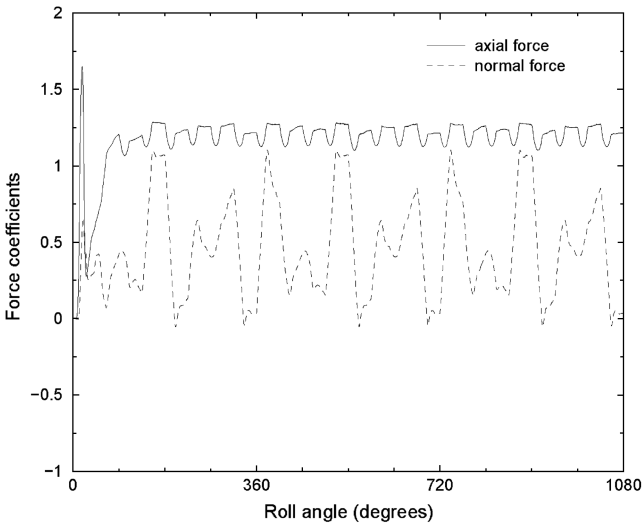

Fig. 4 Convergence of aerodynamic forces using a second-order scheme.

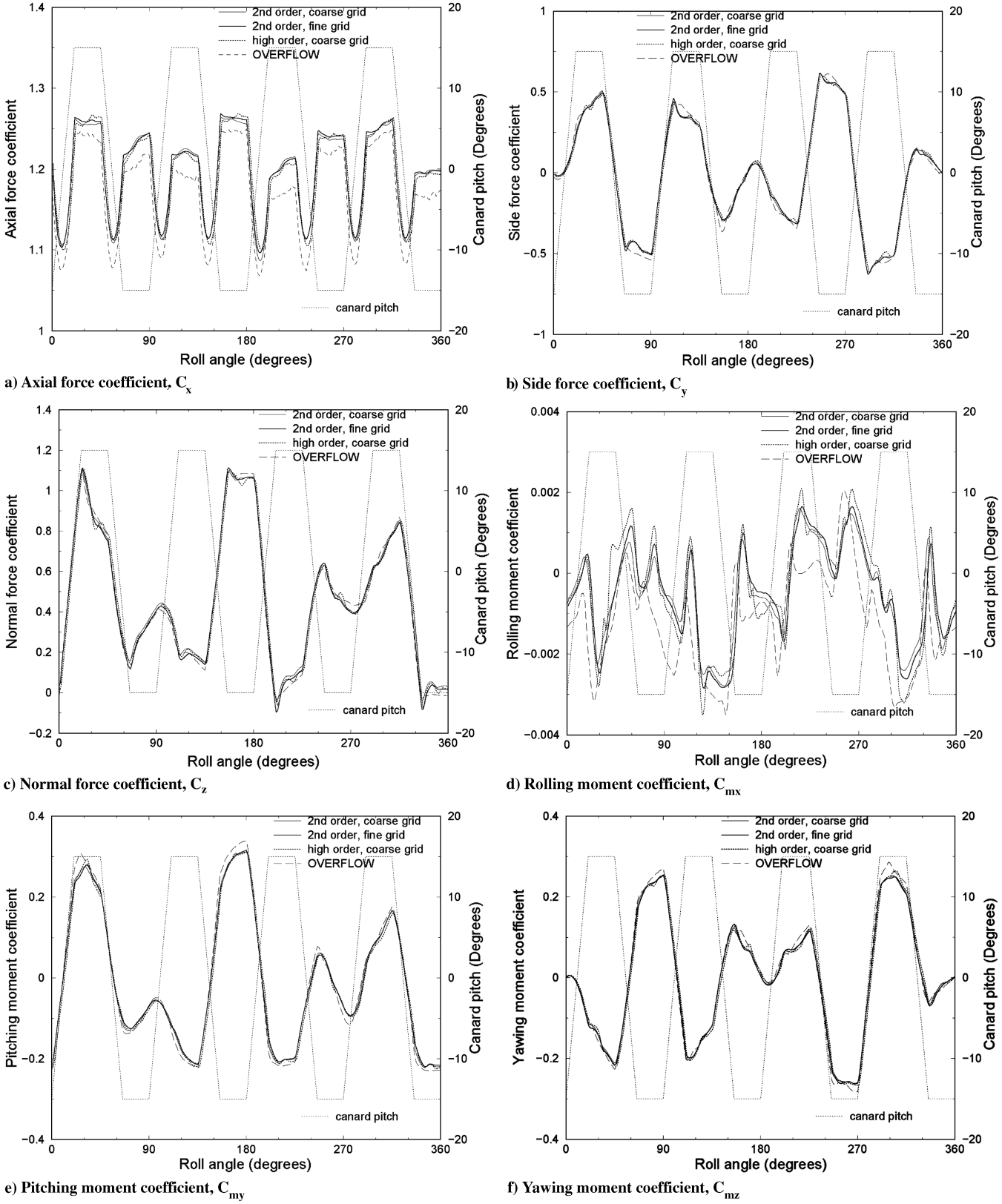

a) Axial force coefficient, C_x

b) Side force coefficient, C_y

c) Normal force coefficient, C_z

d) Rolling moment coefficient, C_{mx}

e) Pitching moment coefficient, C_{my}

f) Yawing moment coefficient, C_{mz}

Fig. 5 Computed force and moment coefficients over one spin revolution.

force and moment coefficients are compared with the benchmark results obtained by OVERFLOW code.

Convergence History

The unsteady time-accurate simulation of the spinning missile was initiated from a uniform flow using second-order temporally accurate, original second-order, and new higher-order flux reconstruction schemes, as described in the previous section. To ensure the temporal accuracy of the unsteady solution, six symmetric Gauss–Seidel relaxations and four Newton subiterations were used per time step. This minimum time step corresponds to 1 deg of roll angle for the missile per time step, which is significantly larger compared to other explicit or semi-implicit methods [1,2]. It seems to provide a

Table 1 Comparison of roll-averaged force and moment coefficients

	Grids (millions)	C_x	C_y	C_z	C_{mx}	C_{my}	C_{mz}
Original scheme	9.26	1.195	0.474	−3.632e − 3	−5.107e − 4	−8.016e − 3	4.420e − 4
Original scheme	17.02	1.197	0.464	−4.493e − 3	−5.226e − 4	−6.639e − 3	−3.286e − 4
New scheme	9.26	1.194	0.468	−2.707e − 3	−4.800e − 4	−1.104e − 2	6.601e − 4
OVERFLOW	41	1.172	0.469	−7.56e − 3	−1.19e − 3	−6.79e − 3	2.80e − 3

balanced need for both temporal resolution and computational efficiency. The simulation showed that the shock waves and canard-induced vortices were formed rather quickly around the missile body at supersonic Mach numbers. The predicted aerodynamic forces and moments were fully converged in about one half-revolution after the simulation was initiated. Figure 4 shows the time history of the axial force and normal force coefficients obtained using the second-order flux scheme on the baseline grid.

The simulation using the higher-order flux reconstruction scheme was restarted from the converged second-order solution using the same solver input parameters. It was found that after only one-third roll revolution (120 deg), the higher-order solution was fully converged, although the simulation was carried out for five revolutions. The current flux reconstruction method was proven to be rather successful in predicting such a complicated and challenging aerodynamic problem. It showed improved numerical accuracy in the smooth region while maintaining the stability of the solution at discontinuities (shocks), which is one of the major difficulties faced by many high-order schemes in practical applications [23].

In terms of the CPU time costs, it was found that the current higher-order implementation only encountered less than a 10% increase in the CPU time compared with the original second-order scheme. It is expected that more overhead of CPU times would occur if Gauss quadrature integration is exactly implemented at the interface of control volumes. There is no memory increase in the current method, since the current higher-order flux reconstruction is based on the primitive variables and their first derivatives, which are readily available in the original second-order scheme.

Unsteady Forces and Moments

One goal of the present study is to investigate the unsteady aerodynamic forces and moments on the spinning missile with dithering canards. Three force coefficients and three moment coefficients are obtained and normalized based the freestream dynamic pressure $Q_\infty = \frac{1}{2}\rho_\infty U_\infty^2$ and the cross-sectional area S_{ref} at maximum body diameter L_{ref}, which can be expressed as

$$C_F = \frac{\text{force}}{Q_\infty S_{\text{ref}}}; \qquad C_M = \frac{\text{moment}}{Q_\infty S_{\text{ref}} L_{\text{ref}}} \tag{10}$$

The moments are calculated about the missile center of gravity.

Figure 5 shows predicted unsteady force and moment coefficients using the original and new higher-order flux reconstruction methods, along with the OVERFLOW results obtained by Nygaard and Meakin [1] for comparison purposes. The canard pitch scheme over a single spin revolution is also indicated in the plots. It should be noted that the OVERFLOW results [1] were obtained using a Chimera overset structured-grid methodology and using an extremely fine spatial and temporal resolution with 41 million grid points and 12,000 time steps per revolution. The current solutions were obtained based on unstructured grids with 9.26 million (coarse) and 17.01 million (fine) grid points and a time resolution of 360 time steps per revolution. Predicted force and moment coefficients indicate that the major aerodynamic characteristics associated with the dithering canards have been captured in all simulations. The forces and moments predicted in the current simulation match very well with the baseline OVERFLOW results, except for the rolling moment coefficients. The rolling moments were found to incur the maximum difference as the canards stay at their extreme pitch angles among solutions. It seemed that predicted axial forces on the current unstructured grids are 2.46% higher than those obtained by OVERFLOW structured-grid results. This may be due to the grid resolution between the two computational meshes. Although no major differences were found on the total axial forces acting on the missile between the original and new flux reconstruction schemes, the componentwise axial forces, especially on the canards, were found to be rather different. This is due to the fact that axial forces and rolling moments are mostly affected by the canard deflecting angle, where the canard-induced vortices predicted by different schemes may impact the missile aerodynamic performance. Table 1 summarizes the roll-averaged mean force and moment values predicted based on the original and the current higher-order schemes on the baseline and fine grids, as well as the OVERFLOW results obtained on an extremely fine mesh.

Pressure and Shock Structures

The supersonic flowfield around the spinning missile is characterized by a bow shock in front of the missile nose and multiple oblique shocks and expansive waves generated by canards, boattails, and tail fins. These shocks and expensive waves directly interact with the body boundary layers and, most important, the vortices induced by the canards. Figure 6 shows an overall flow structure of the pressure contours for the missile configuration obtained using the higher-order flux scheme, which illustrates various shocks and expansive waves. As previously described, the high-order flux discretization method presented in this work is intended to capture the strong discontinuity (shocks) while preserving the higher-order accuracy in the smooth region (vortices). Figure 7 compares the pressure contours near the missile nose region obtained by the original and current methods. There is only slight improvement to the predicted bow shock thickness using the current higher-order flux reconstruction compared to the original second-order method, which is not surprising, due to the use of the limiter-detector technique [10]. The limiter-detector technique maintains the numerical stability at

Fig. 6 Predicted instantaneous pressure on missile surface and *x-y* plane.

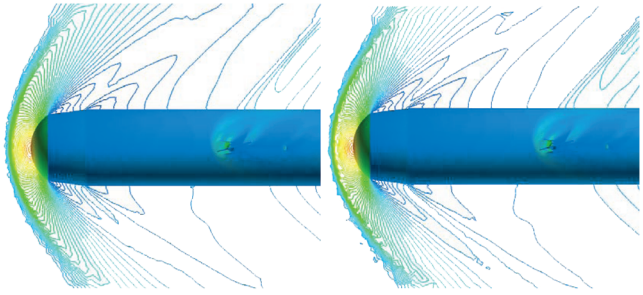

Fig. 7 Predicted bow shocks and pressure contours on the nose and canards.

discontinuity by reducing the order of accuracy of the scheme, but it improves the prediction accuracy in the smooth region only. However, the pressure contours obtained by the higher-order method show more details in the canard region compared to the original second-order result.

Canard Vortex Convection

A dominant flow feature of this spinning missile is the canard-induced vortices, which introduce very complicated and unsteady interactions with shocks, expansion waves, and body boundary layers. Each canard induces a pair of counter-rotating vortices. The one at the tip of the canard is called the outboard vortex, and the one at the root of the canard is called the inboard vortex [1]. Since the inboard vortex is closer to the missile body, its development and convection to downstream has a larger impact on the missile aerodynamics. Therefore, accurate prediction of the vortices is very important to understand the complex, unsteady, and interactional flowfield of the spinning missile. However, most conventional Eulerian-based numerical methods suffer excessive numerical diffusion, resulting in quick smearing of the vortex strength predicted in the flowfield. The higher-order flux scheme developed in the present study is intended to reduce the excessive numerical diffusion and to better preserve the vortex strength and convection in the flowfield. It can also be used in combination with the grid adaptation and/or local grid refinement for an even better effect, although it is rather expensive and/or difficult to implement for large-scale, unsteady, and parallel computations on unstructured grids, owing to the dynamic memory allocation and load-balancing issues.

In the context of fluid dynamics, a measure to the strength of vortices is called helicity, which defines the helical motion of the fluid. When a parcel of fluid is undergoing a rotating motion about an axis parallel to the direction of motion, it will create helicity. Helicity is simply the dot product of the velocity and the vorticity vector:

$$H = \int u \cdot (\nabla \times u) \mathrm{d}^3 r \tag{11}$$

where $\boldsymbol{u}$ is the local flow velocity and r is the local distance for the volume integration. An advantage of using the helicity vs other quantities (such as vorticity) to represent vortical flows is that it

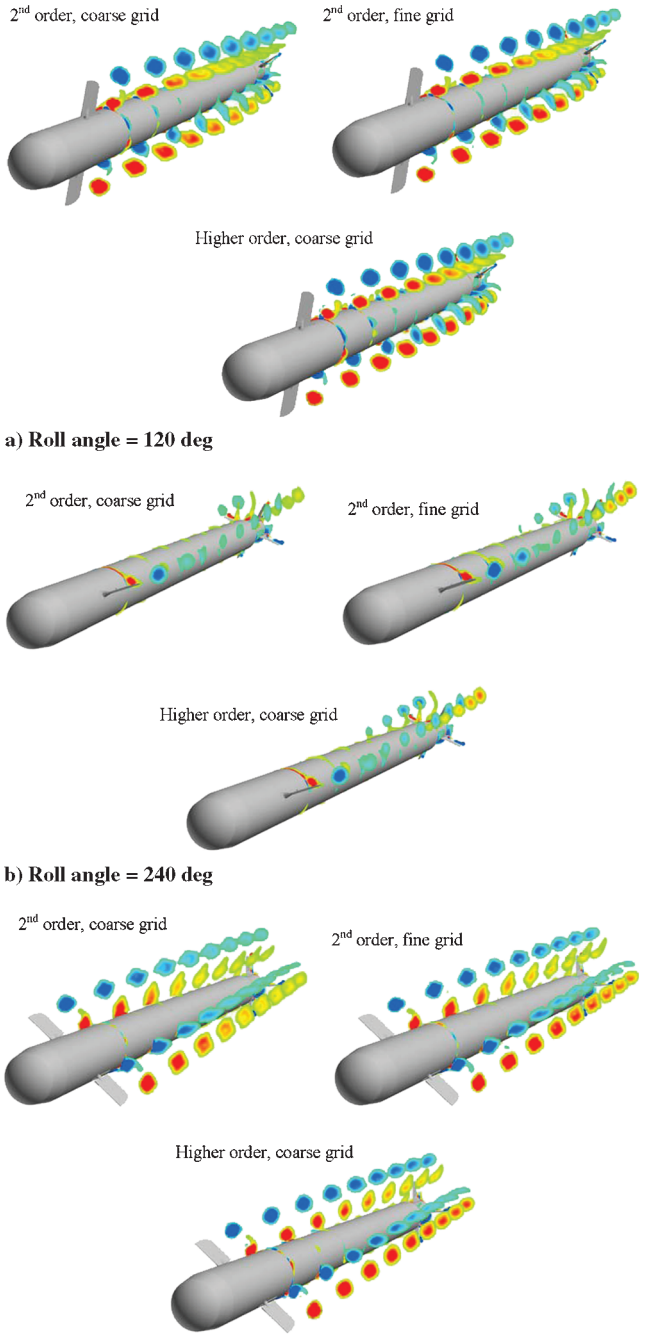

a) Roll angle = 120 deg

b) Roll angle = 240 deg

c) Roll angle = 360 deg

Fig. 8 Helicity counters of canard-induced vortices at 120, 240, and 360 deg roll angles.

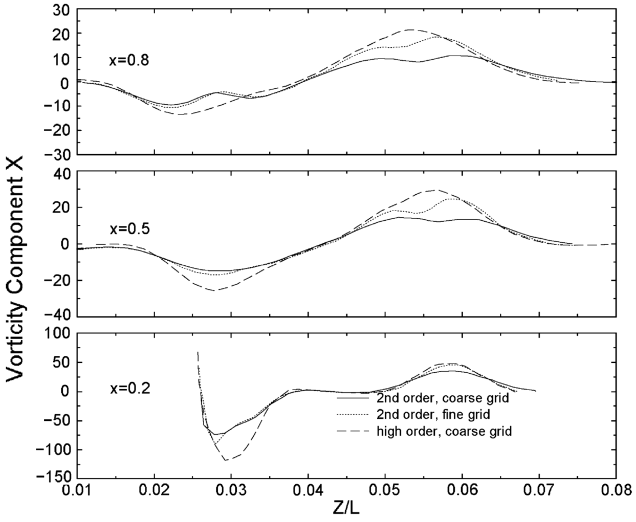

a) Variation of x-vorticity components through inboard and outboard vortex cores

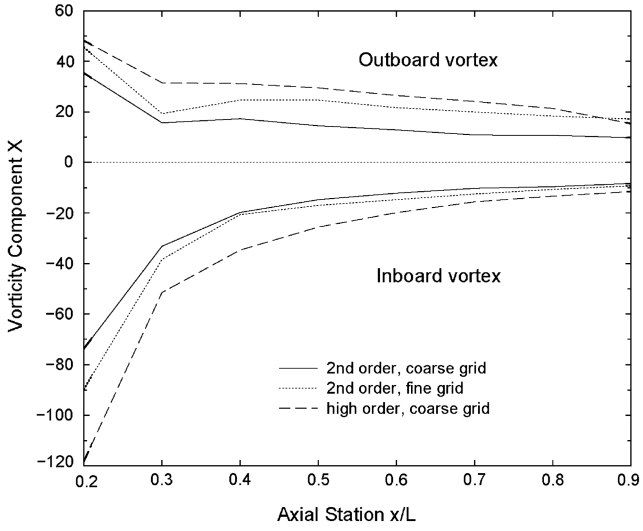

b) Vortex decay along the missile axial direction

Fig. 9 Predicted x component vorticity of inboard and outboard vortices.

shows not only the strength of vortices but also the direction of the vortex rotation. As shown in the following Fig. 8, the red color indicates a positive helicity, which is rotating clockwise when viewed from the missile nose to tail. The blue color indicates negative helicity, for which the rotation is counterclockwise. The missile body is also rotating clockwise when viewed from the nose to tail.

Figure 8 shows the comparisons of the instantaneous helicity contours predicted by the original and the current higher-order discretization method at three different missile roll angles (120, 240, and 360 deg). The initial missile orientation is at the 360 deg roll angle representing two canards in horizontal position and the freestream approaching at a 3 deg angle of incidence. The helicity contours were calculated at various cutting planes along the free-stream direction, starting right behind the canard surfaces toward the end of the missile body. Figure 8 reveals the dynamic nature and vortical flow development associated with the spinning missile. Both inboard and outboard canard vortices move along with the dithering canards and rotate with the spinning missile. The canard-induced vortices remain strong at most positions of the missile rolling motion. The weakest vortices occur as the canard flaps its pitch angle from positive to negative, or vice versa, in which the induced vortices change the direction of rotation. At all three missile orientations, the solution predicted by the higher-order method on the baseline coarse grid showed less numerical dissipation and better vortex convection to the downstream compared to the original second-order solutions. By increasing the grid resolution, the second-order scheme was able to improve the vortex prediction, but not to the same level as the higher-order solution. This comparison indicates that the savings in computational time is at least 50% by using the new higher-order flux scheme over the original second-order scheme for the current simulations, since the refined grid has about twice the number of nodes compared to the baseline coarse grid.

More quantitative comparisons were carried out for the flow vorticity calculated using the original and the current higher-order schemes. Figure 9a shows the x component of the vorticity calculated at three axial stations at $x/L = 0.2$, 0.5, and 0.8, where L is the missile body length. The inboard vortex has a negative x vorticity, and the outboard vortex has a positive x vorticity. The negative perk value indicates the inboard vortex core, and the positive perk value matches the outboard vortex core. For both inboard and outboard vortices, the predicted vortex strength with the original method cannot match that in the current higher-order solution, even on the refined grid. The same conclusion is true with the vorticity variation along the axial direction of the missile body, as shown in Fig. 9b. The strength of the inboard vortex is higher than that of the outboard vortex, and the inboard vortex decays faster than the outboard vortex because of the interference with the missile body. The vorticity

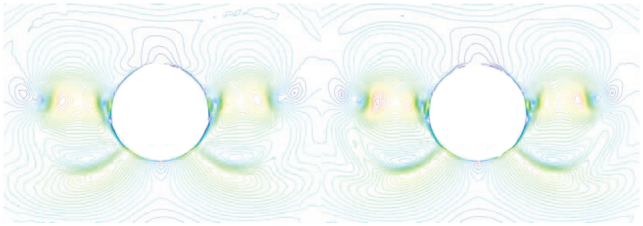

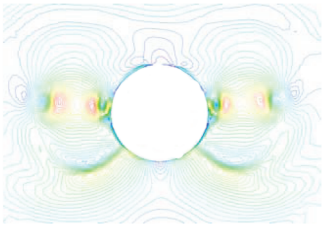

Fig. 10 Comparison of crossflow velocity contours at section $x/L = 0.2$.

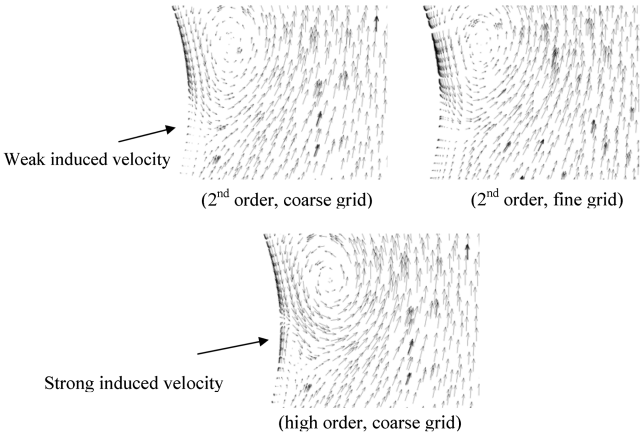

Fig. 11 Comparison of crossflow velocity vectors at section $x/L = 0.2$.

variation shows a higher level of numerical dissipation in the original second-order solution, which implies that an even more refined mesh and more points should be used to achieve the same level of vortex prediction as with the current higher-order method. This clearly demonstrates the efficacy and improvement of the current higher-order method in predicting vortex-dominant flows, even in the presence of strong shocks.

Vortex and Boundary-Layer Interaction

As has been discussed in the previous sections, the canard-induced vortices (in particular, the inboard one) have strong interactions with the missile body and tail fins, which thus changes the boundary-layer profile. The use of the higher-order flux scheme not only improves the prediction of the vortex strength and convection but also helps capture the fine details of the flowfield, which has been omitted or dissipated in the second-order solutions. Figure 10 shows the instantaneous crossflow velocity contours (in the y-z plane) at the section of $x/L = 0.2$ measured from the nose of the missile body, or a 0.05 body distance behind the canard trailing edge. The missile airframe orientation is at a 360 deg roll angle. It is seen that both inboard and outboard vortices induced by canards have been predicted in the original and the current higher-order solutions. However, the higher-order result reveals refined flow details near the missile body surface, as the canard-induced vortices penetrate into the boundary layers and change the velocity profile. Induced velocity near the missile body seems to be stronger in the higher-order solution than that in the original second-order solutions (on both coarse- and fine grids), as shown in Fig. 11. Since the change of velocity profile in the boundary layers may change the skin fraction acting on the body, improved prediction of vortices in the field may also impact the prediction of aerodynamic forces and moments (in particular, in the Navier–Stokes viscous simulations). In fact, although not seen in the total axial force of the missile body (Fig. 5a), the componentwise axial force on the canards does show the difference among the original second-order and new higher-order solutions, due to the change of velocity profiles in the boundary layer.

Conclusions

Unsteady viscous flow simulations of a spinning missile with dithering canards have been carried using the original second-order and new higher-order flux reconstruction schemes. A novel approach has been introduced and investigated for the piecewise quadratic polynomial reconstruction of primitive variables for developing the higher-order discretization scheme on unstructured grids. The efficacy and robustness of the new higher-order scheme has been demonstrated in the simulation of a spinning missile with dithering canards, which indicated an improved numerical accuracy in the smooth vortical flow region while maintaining the stability at the discontinuity such as shocks. This new method, although yet to be verified for its formal order of accuracy, has shown the great potential for predicting practical and challenging aerodynamic problems, such

as the spinning missile that involves fast roll motion with dithering canards, strong vortex convection, multiple shocks and expansive waves, and interactions with the boundary layers. The following concluding remarks are given in the present study:

1) A new flux reconstruction method has been introduced and demonstrated for the improved numerical accuracy and less numerical dissipation in the smooth region, while maintaining the stability of the solver at discontinuities, a key attribute to be applied to complex and challenging aerodynamic problems.

2) Grid resolution studies indicated at least 50% savings in computational time may be achieved by using the current higher-order discretization method vs the original second-order method to obtain the same level of numerical accuracy for vortex-dominant flows.

3) Each dithering canard introduced a pair of inboard and outboard vortices, which moved along with the canard and changed the direction of rotation back and forth as the dithering canard flapped the pitch angle. These canard-induced vortices had a strong impact on the boundary-layer profiles of the spinning missile.

4) Improved prediction of induced vortices, shocks, and their interaction with the boundary layer using the high-order approach provided better understanding of the complex aerodynamic characteristics associated with the spinning missile with dithering canards.

References

[1] Nygaard, T. A., and Meakin, R. L., "An Aerodynamic Analysis of a Spinning Missile with Dithering Canards," 20th AIAA Applied Aerodynamics Conference, St. Louis, MO, AIAA Paper 2002-2799, June 2002.

[2] Nygaard, T. A., and Meakin, R. L., "Aerodynamic Analysis of a Spinning Missile with Dithering Canards," *Journal of Spacecraft and Rockets*, Vol. 41, No. 5, Sept.–Oct. 2004, pp. 726–734. doi:10.2514/1.13075

[3] Blades, E. L., Marcum, D. L., and Mitchell, B., "Simulation of Spinning Missile Flow Fields using U^2NCLE," 20th AIAA Applied Aerodynamics Conference, St. Louis, MO, AIAA Paper 2002-2797, June 2002.

[4] Blades, E. L., and Marcum, D. L., "Numerical Simulation of a Spinning Missile with Dithering Canards Using Unstructured Grids," *Journal of Spacecraft and Rockets*, Vol. 41, No. 2, March–April 2004, pp. 248–256. doi:10.2514/1.9197

[5] Blades, E. L., and Marcum, D. L., "A Sliding Interface Method for Unsteady Unstructured Flow Simulations," *International Journal for Numerical Methods in Fluids*, Vol. 53, No. 3, 2007, pp. 507–529. doi:10.1002/fld.1296

[6] Sheng, C., Wang, X., Hughson, M., and Marcum, D., "Unsteady Navier–Stokes Simulations of a Canard Controlled Missile Configuration," 26th AIAA Applied Aerodynamics Conference, Honolulu, HI, AIAA Paper 2008-7324, Aug. 2008.

[7] Sheng, C., Newman, J., III, Remotigue, M., Chen, J. P., Marcum, D., and Whitfield, D., "Development of Unstructured Computational Capabilities Applicable to MSU TURBO with an Arbitrary Mach Number Algorithm," Mississippi State Univ., Rept. MSSU-COE-ERC-02-16, Mississippi State, MS, Oct. 2002.

[8] Sheng, C., and Wang, X., "Characteristic Variable Boundary Conditions for Arbitrary Mach Number Algorithm in Rotating Frame," 16th AIAA Computational Fluid Dynamics Conference, Orlando, FL, AIAA Paper 2003-3976, June 2003.

[9] Sheng, C., and Narramore, J., "Unsteady Simulations of Bell-Agusta 609 Rotor with Higher Harmonic Oscillation," *Journal of Aircraft*, Vol. 45, No. 3, May–June 2008, pp. 971–980. doi:10.2514/1.32877

[10] Nejat. A., and Ollivier-Gooch, C., "A High-Order Accurate Unstructured Finite Volume Newton-Krylov Algorithm of Inviscid Compressible Flows," *Journal of Computational Physics*, Vol. 227, No. 4, 2008, pp. 2582–2609. doi:10.1016/j.jcp.2007.11.011

[11] "Defensive Missile Wind Tunnel Test for the Validation and Verification of CFD codes," Dynetics, Inc., TR PO 40725, Huntsville, AL, Jan. 2002.

[12] Marcum, D. L., and Gaither, J. A., "Mixed Element Type Unstructured Grid Generation for Viscous Flow," 14th AIAA Computational Fluid Dynamics Conference, Norfolk, VA, AIAA Paper 99-325A, 1999.

[13] *SolidMesh: 3D User's Manual* [online manual], Mississippi State Univ., Mississippi State, MS, 2009, http://www.simcenter.msstate.edu/simcenter/docs/solidmesh/ [retrieved Nov. 2009].

[14] Briley, W. R., Taylor, L. K., and Whitfield, D. L., "High-Resolution Viscous Flow Simulations at Arbitrary Mach Number," *Journal of Computational Physics*, Vol. 184, No. 1, 2003, pp. 79–105. doi:10.1016/S0021-9991(02)00018-9

[15] Anderson, W. K., and Bonhaus, D. L., "Implicit Upwind Algorithms for Computing Turbulent Flows on Unstructured Grids," *Computers and Fluids*, Vol. 23, No. 1, 1994, pp. 1–21. doi:10.1016/0045-7930(94)90023-X

[16] Barth, T., and Frederickson, P., "Higher Order Solution of the Euler Equations on Unstructured Grid Using Quadratic Reconstruction," 28th Aerospace Sciences Meeting, AIAA Paper 90-0013, Reno, NV, Jan. 8–11.

[17] Mahesh, K., "A Family of High-Order Finite Difference Schemes with Good Spectral Resolution," *Journal of Computational Physics*, Vol. 145, No. 1, 1998, pp. 332–358. doi:10.1006/jcph.1998.6022

[18] Cockburn, B., and Shu, C., "The Runge-Kutta Discontinuous Galerkin Method for Conservation Laws V: Multidimensional System," *Journal of Computational Physics*, Vol. 141, No. 2, 1998, pp. 199–224. doi:10.1006/jcph.1998.5892

[19] Tang, T., and Li, M., "A Compact Fourth-Order Finite Difference Scheme for Unsteady Viscous Incompressible Flows," *Journal of Scientific Computing*, Vol. 16, No. 1, March 2001, pp. 29–45. doi:10.1023/A:1011146429794

[20] Jiang, G., and Shu, C., "Efficient Implementation of Weighted ENO Schemes," *Journal of Computational Physics*, Vol. 126, No. 1, 1996, pp. 202–228. doi:10.1006/jcph.1996.0130

[21] Wang, Z., Zhang, L., and Liu, Y., "High-Order Spectral Volume Method for 2D Euler Equations," 16th AIAA Computational Fluid Dynamics Conference, AIAA Paper 2003-3534, Orlando, FL, 23–26 June 2003.

[22] Luo, H., Baum, J., and Lohner, R., "A Hermite WENO-Based Limiter for Discontinuous Galerkin Method on Unstructured Grids," *Journal of Computational Physics*, Vol. 225, No. 1, July 2007, pp. 686–713.

[23] Wang, J. Z., "Recent Progresses and Remaining Challenges in Adaptive High-Order CFD Method—A Survey on High-Order Methods," *19th AIAA Computational Fluid Dynamics Conference*, San Antonio, TX, June 2009.

[24] Spalart, P., and Allmaras, S., "A One-equation Turbulence Model for Aerodynamic Flows," 30th AIAA Aerospace Sciences Meeting, Reno, NV, AIAA Paper 92-0439, Jan. 1992.

R. Cummings
Associate Editor